

Data-driven feedback linearisation using model predictive control

Merijn Floren^{a,*}, Koen Classens^b, Tom Oomen^b, Jean-Philippe Noël^a

^a*KU Leuven, Department of Mechanical Engineering, Mecha(tro)nic System Dynamics Division, Celestijnenlaan 300, 3001 Leuven, Belgium*

^b*Eindhoven University of Technology, Department of Mechanical Engineering, Control Systems Technology Group, PO Box 513, 5600 MB Eindhoven, The Netherlands*

Abstract

Linearising the dynamics of nonlinear mechanical systems is an important and open research area. In this paper, we adopt a data-driven and feedback control approach to tackle this problem. A model predictive control architecture is developed that builds upon data-driven dynamic models obtained using nonlinear system identification. The overall methodology shows a high degree of performance combined with significant robustness against imperfect modelling and extrapolation. These findings are demonstrated using large set of synthetic experiments conducted on a asymmetric Duffing oscillator and using an experimental prototype of a high-precision motion system.

Keywords: feedback linearisation, nonlinear mechanical systems, nonlinearity, model predictive control, data-driven modelling, nonlinear system identification.

1. Introduction

Following the rapid development of our modern society, engineering systems are becoming increasingly complex. In mechanics, this complexity translates in most applications in the appearance of nonlinear behaviours. Consider, for instance, the aerospace sector, where the demands for reduced fuel consumption, increased payload and increased flight range are accommodated by designing ever lighter aircraft structures [1]. An inevitable result of this quest for squeezing the structural weight is the activation of pronounced nonlinear effects [2]. If nonlinear dynamic behaviours can only be accurately captured by nonlinear models, in terms of control engineering however, it is much more appealing to work with linear models. In order to meet the engineers' desire, research efforts amongst a range of disciplines have focused on linearising nonlinear systems using feedback control.

Fig. 1 illustrates the general working principle of feedback linearisation for a single-input single-output (SISO) nonlinear system. In essence, the plant input $u(t)$ is modified, through a choice of a nonlinear state feedback control law, such that the input-output (IO) relation between the new outer-loop input $v(t)$ and system output $y(t)$ is linear. This linear relation holds for the entire specified operating range, meaning that the IO response of an equivalent linear time-invariant (LTI) system is obtained. Subsequently, standard linear control techniques can be used to design an outer-loop controller that is stable over the operating range and exhibits the same transient and steady-state behaviours for different set-points, *e.g.*, the proportional-integral-derivative (PID) controller of Fig. 1.

The commonly used technique for feedback linearisation is the analytical approach based on Lie algebra [3–5]. This approach intends to find a direct linear relationship between the system output and a new control input, and eventually transforms the original system into a chain of integrators. In a recent study [6], analytical feedback linearisation was applied in combination with an outer-loop linear quadratic regulator in order to control the desired altitude and attitude levels of a quadrotor. In [7], the same approach was applied to linearise the dynamics of a nonlinear wind

*Corresponding author

Email addresses: merijn.floren@kuleuven.be (Merijn Floren), k.h.j.classens@tue.nl (Koen Classens), t.a.e.oomen@tue.nl (Tom Oomen), jp.noel@kuleuven.be (Jean-Philippe Noël)

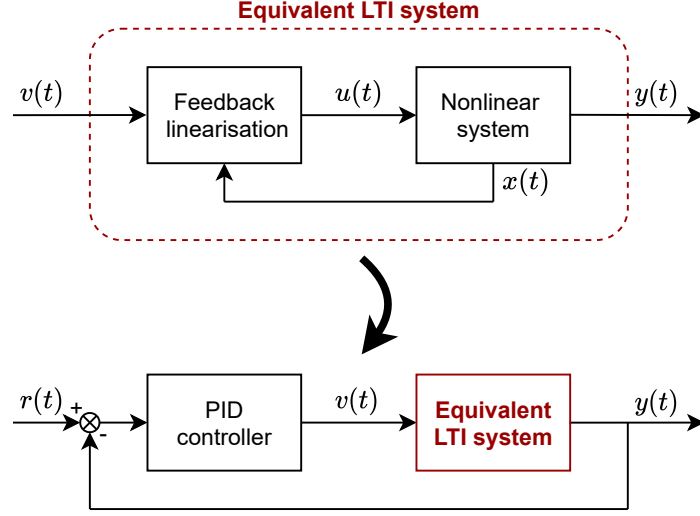


Figure 1: Block diagram illustrating the simplified working principle of feedback linearisation. In a first step, the plant input $u(t)$ is modified such that for the new input $v(t)$ a linear output response is obtained. In a second step, the equivalent LTI system can be integrated in any linear outer-loop control scheme, in this example a classical PID feedback loop with reference tracking.

turbine, after which the obtained LTI system supported the design of an outer-loop model-based controller. A comparison between analytical feedback linearisation and gain scheduling was drawn in [8], where feedback linearisation in combination with a PI controller showed significant improvement in terms of performance and robustness in the control of a nonlinear boiler-turbine unit. In the authors' view, the promise of feedback linearisation based on Lie algebra has never been solidly realised since its inception in the early eighties. We explain this by the fact that the underlying methodology assumes the availability of a reliable nonlinear first-principle-based model, that is resource-consuming to develop, bound to a limited accuracy, and inefficient in a control context.

In this paper, a novel and effective approach towards feedback linearisation is presented. The first novelty is that the models that we exploit are obtained by exclusively processing IO data, thus having the advantage that complex systems can be represented without addressing first-principle methods. Furthermore, the linearising controller exploits model predictive control (MPC), that is robust to model uncertainty and imperfect state information. The focus of this work is on nonlinear mechanical systems. Many of such systems, albeit in an implicit form, can be modelled as LTI systems with a negative feedback path containing static nonlinearities [9], as illustrated in Fig. 2. Consider, for instance, the mass-spring-damper system with a cubic spring nonlinearity

$$m\ddot{y}(t) + c_l\dot{y}(t) + k_ly(t) + k_c y^3(t) = u(t), \quad (1)$$

where the output $y(t)$ is the displacement of the mass m , and the input $u(t)$ is a force exiting the mass. Moreover, c_l and k_l are the linear damping and stiffness constants, respectively; k_c is the cubic spring coefficient and the over-dot indicates a derivative with respect to the time variable t . The dynamics can easily be rewritten to obey the structure of Fig. 2, as

$$m\ddot{y}(t) + c_l\dot{y}(t) + k_ly(t) = u(t) - k_c y^3(t), \quad (2)$$

suggesting that the cubic spring nonlinearity acts as an additional input to the underlying linear system. A system that can be modelled in this manner allows for a more careful selection of the nonlinear basis functions for system identification, since it is known that the nonlinearities are functions of the outputs only. Furthermore, these models clearly distinguishes the underlying linear dynamics in the feedforward path from the undesirable nonlinearities in the feedback branch. In the case of vibrating systems, it is known that the linear dynamics are stable and contain the important vibration properties of the system, namely its linear modal properties. In this study, we treat systems can be represented by the model structure of Fig. 2.

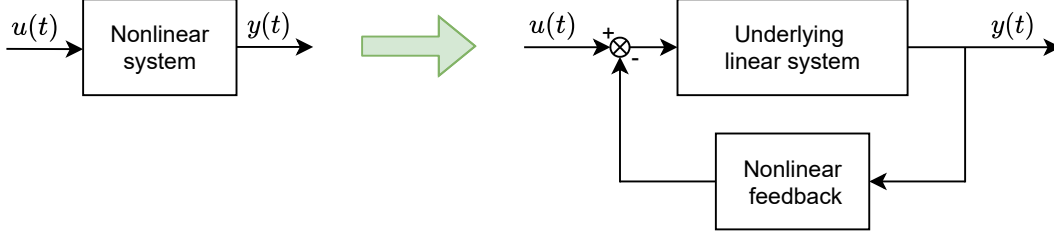


Figure 2: Illustration of the model structure adopted in this work. A nonlinear mechanical system is modelled as an underlying linear system with a static nonlinear output function wrapped around it in feedback.

In summary, the four main contributions of the paper are:

- the development of a new framework that exploits data-driven models and robust MPC towards linearising the IO response of nonlinear mechanical systems.
- the preservation in this framework of the underlying LTI response of the system, or alternatively, of its linear vibration properties.
- the quantification of the linearising performance over a wide range of frequencies by means of a nonparametric nonlinear distortion analysis.
- the validation of the proposed framework using an experimental academic setup.

The paper is organised as follows: firstly, Section 2 presents the details of the proposed approach; this includes both the control design method as well as the data-driven modelling and analysis tools. Section 3 studies a rich set of simulation examples in order to demonstrate the performance and robustness properties of the introduced framework. In Section 4, the complete control structure is validated by means of experimental tests on a prototype of a high-precision motion system. Finally, conclusions are drawn and recommendations for future works are discussed in Section 5.

2. Data-driven feedback linearisation framework

This section introduces the methodologies that subtend the introduced linearisation framework. First, the novel control strategy is described in detail. Next, a brief overview is given regarding the data-driven modelling and analysis tools.

2.1. Control design

The dynamic models considered in this work are purely data-driven. More specifically, the focus is on discrete-time SISO polynomial nonlinear state-space models, defined at time instant $k \in \mathbb{N}$ as

$$\begin{cases} x(k+1) = \mathbf{A}x(k) + \mathbf{B}u(k) + \mathbf{E}\zeta(y(k)) \\ y(k) = \mathbf{C}x(k), \end{cases} \quad (3)$$

where $\mathbf{A} \in \mathbb{R}^{n \times n}$, $\mathbf{B} \in \mathbb{R}^{n \times 1}$ and $\mathbf{C} \in \mathbb{R}^{1 \times n}$ are the linear state, input, and output matrices, respectively, and with n being the model order. Furthermore, $x(k) \in \mathbb{R}^n$ is the state vector, $u(k) \in \mathbb{R}$ the plant input and $y(k) \in \mathbb{R}$ the plant output; $\zeta(y(k)) \in \mathbb{R}^s$ is a vector containing the s monomial terms of the nonlinear polynomial basis function, with $\mathbf{E} \in \mathbb{R}^{n \times s}$ the associated coefficient matrix. The model in the form of (3) corresponds to the structure schematised in Fig. 2, with $\mathbf{E}\zeta(y(k))$ being the undesired static nonlinearity in the feedback loop.

This nonlinearity is to be eliminated from the IO response, while the underlying linear dynamics are preserved. To this end, an internal reference tracking framework is proposed that follows a one-step-ahead reference for any outer-loop input $v(k)$. This reference point, which is generated online at any time instant k , is the one-step-ahead

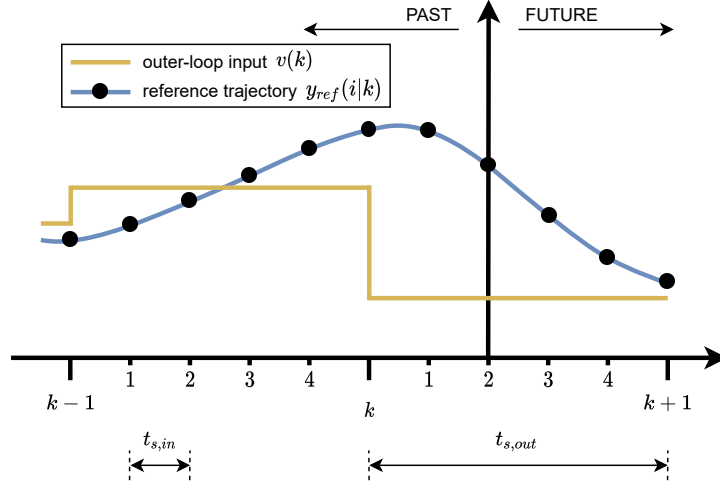


Figure 3: Illustration of the proposed MPC solution with online reference generation and dynamic prediction horizon length. The notation $y_{ref}(i|k)$ indicates the output reference point at the i th inner-loop sub-sample of the k th outer-loop time instant. At the current time instant, there are 3 out of 5 future references available. The number of available references reduces to 1 as time progresses up until time $k + 1$, where a new outer-loop input will allow for the generation of 5 new reference points.

output response of the desirable linear part of the model to $v(k)$. In mathematical terms, the one-step-ahead reference point at time instant k is defined as follows

$$\begin{cases} x_{ref}(k+1) = \mathbf{A}x_{ref}(k) + \mathbf{B}v(k) \\ y_{ref}(k+1) = \mathbf{C}x_{ref}(k+1), \end{cases} \quad (4)$$

where $x_{ref}(k+1)$ is the state reference and $y_{ref}(k+1)$ is the output reference to be tracked. So, a controller that is capable of perfectly tracking this one-step-ahead reference point at any time k for any input $v(k)$, generates an IO relation between $v(k)$ and $y(k)$ that is governed by the linear part of the identified model.

An MPC [10–13] controller is used to achieve the tracking objective. In the described form, the prediction horizon is equal to 1. Although such a short prediction horizon is often seen in the field of power electronics [14–17], it is almost never used for systems with slower dynamics. For the latter systems, in order to obtain a stabilising MPC controller, the sample time must be sufficiently low while the prediction horizon must be sufficiently high. Common practice for improving performance is to decrease the sample time and/or increase the prediction horizon, at the cost of computational complexity. With this in mind, we propose a control architecture where the inner-loop (the linearising MPC) runs at a higher sample rate than the outer-loop (any linear controller). In particular, this means that the outer-loop input signal $v(k)$ is supplied at a lower rate than the execution rate of the MPC. In this way, the one-step-ahead reference point can be reached by following a reference trajectory, with smaller intermediate time steps. By doing so, the sample time is decreased whilst the prediction horizon length is increased. A consequence of the proposed solution is that the prediction horizon has a *dynamic* length, as a result of the ever-changing number of available reference points. This dynamic horizon strategy is illustrated in Fig. 3. More generally, the future references according to Fig. 3 are generated as

$$\begin{cases} x_{ref}(i+1|k) = \mathbf{A}x_{ref}(i|k) + \mathbf{B}v(i|k) \\ y_{ref}(i+1|k) = \mathbf{C}x_{ref}(i+1|k), \end{cases} \quad (5)$$

where $x_{ref}(i+1|k)$ and $y_{ref}(i+1|k)$ are the future state and output sub-reference points based on the outer-loop input $v(i|k) = v(k)$, for $i \in \{0, \dots, N_{p,\max} - 1\}$, with $N_{p,\max} = t_{s,out}/t_{s,in} \in \mathbb{N}$. Moreover, note that \mathbf{A} and \mathbf{B} here correspond to sample time $t_{s,in}$ as opposed to $t_{s,out}$ in (4).

Typically, MPC is used to track state references while at the same time assuring that constraints on the input and the states are not violated. In this study however, the states are of minor importance since they do not have a physical meaning. Constraint bounds on the input could be more of an interest. Yet, we choose not to incorporate them since this would require an online optimisation problem to be executed at every time step, leading to a significant increase in computational load.

The proposed linearising MPC controller has integral action, in the sense that robust convergence can be achieved in case of modelling errors and imperfect state information. To obtain this, the original model is augmented such that the state equation also contains the current measured output, as inspired by the velocity form approach in [18–20]. However, the velocity form approach is designed for linear systems, whereas a full nonlinear model is considered here. By utilising the available information of the reference signal, the nonlinear MPC problem can be transformed into a conventional linear MPC with a disturbance matrix.

Consider again the n th order SISO discrete-time fully nonlinear model

$$\begin{cases} x(i+1|k) = \mathbf{A}x(i|k) + \mathbf{B}u(i|k) + \mathbf{E}\zeta(y(i|k)) \\ y(i|k) = \mathbf{C}x(i|k), \end{cases} \quad (6)$$

corresponding to sample time $t_{s,in}$. In order to augment the state space, the following relations are defined:

$$\begin{cases} \Delta x(i|k) &:= x(i|k) - x(i-1|k) \\ \Delta u(i|k) &:= u(i|k) - u(i-1|k) \\ \Delta \zeta(y(i|k)) &:= \zeta(y(i|k)) - \zeta(y(i-1|k)). \end{cases} \quad (7)$$

Next, the state-space model (6) in augmented form writes

$$\begin{cases} \bar{x}(i+1|k) = \underbrace{\begin{bmatrix} \mathbf{A} & \mathbf{0}_{n \times 1} \\ \mathbf{C}\mathbf{A} & 1 \end{bmatrix}}_{\bar{\mathbf{A}}} \bar{x}(i|k) + \underbrace{\begin{bmatrix} \mathbf{B} \\ \mathbf{C}\mathbf{B} \end{bmatrix}}_{\bar{\mathbf{B}}} \Delta u(i|k) + \underbrace{\begin{bmatrix} \mathbf{E} \\ \mathbf{C}\mathbf{E} \end{bmatrix}}_{\bar{\mathbf{E}}} \Delta \zeta(y(i|k)) \\ y(i|k) = \underbrace{\begin{bmatrix} \mathbf{0}_{1 \times n} & 1 \end{bmatrix}}_{\bar{\mathbf{C}}} \bar{x}(i|k), \end{cases} \quad (8)$$

where $\bar{x}(i|k) = [\Delta x(i|k)^\top \ y(i|k)]^\top$. At time $t(i|k)$, the predicted future outputs of (8) over prediction horizon N_p , *i.e.*,

$$Y_k = [y(i+1|k), \dots, y(i+N_p|k)]^\top \in \mathbb{R}^{N_p}, \quad (9)$$

is a function of the current state, input sequence and disturbance sequence; it is defined as

$$Y_k = S_x \bar{x}(i|k) + S_u \Delta U_k + S_g \Delta G_k, \quad (10)$$

where S_x , S_u and S_g are auxiliary matrices that describe the evolution of the states and output over the prediction horizon. A detailed derivation of these matrices is provided in Appendix A. Furthermore,

$$\Delta U_k = \begin{bmatrix} \Delta u(i|k) \\ \vdots \\ \Delta u(i+N_p-1|k) \end{bmatrix} \in \mathbb{R}^{N_p}; \quad \Delta G_k = \begin{bmatrix} \Delta \zeta(y(i|k)) \\ \vdots \\ \Delta \zeta(y(i+N_p-1|k)) \end{bmatrix} \in \mathbb{R}^{sN_p}, \quad (11)$$

where ΔU_k is the vector to be optimised and ΔG_k is the vector of future disturbances. Here, the word disturbance is used because the elements of ΔG_k cannot be controlled. In fact, there is a conflicting situation between ΔG_k and Y_k since they are mutually dependent. Fortunately, ΔG_k can very well be estimated in advance, by substituting the

available reference information of (5) for the future outputs. Thus, the estimate of ΔG_k becomes

$$\Delta \tilde{G}_k = \begin{bmatrix} \zeta(y(i|k)) - \zeta(y(i-1|k)) \\ \zeta(y_{ref}(i+1|k)) - \zeta(y(i|k)) \\ \vdots \\ \zeta(y_{ref}(i+N_p-1|k)) - \zeta(y_{ref}(i+N_p-2|k)) \end{bmatrix}. \quad (12)$$

By doing so, it is assured that Y_k can be computed solely based on available data and the to be optimised input sequence ΔU_k .

Next, the following MPC cost function is proposed

$$J = (Y_k - Y_{k,ref})^\top \Omega (Y_k - Y_{k,ref}) + \Delta U_k^\top \Psi \Delta U_k, \quad (13)$$

where

$$\Omega = \begin{bmatrix} Q & 0 & \cdots & 0 \\ 0 & Q & \cdots & 0 \\ \vdots & \vdots & \ddots & \vdots \\ 0 & 0 & \cdots & Q \end{bmatrix} \in \mathbb{R}^{N_p \times N_p}; \quad \Psi = \begin{bmatrix} R_\Delta & 0 & \cdots & 0 \\ 0 & R_\Delta & \cdots & 0 \\ \vdots & \vdots & \ddots & \vdots \\ 0 & 0 & \cdots & R_\Delta \end{bmatrix} \in \mathbb{R}^{N_p \times N_p}, \quad (14)$$

with Q being a positive scalar penalising any deviation from the reference and R_Δ being a positive scalar penalising the rate of change of the plant input. These values are typically chosen following performance specifications. Moreover, from (5),

$$Y_{k,ref} = [y_{ref}(i+1|k), \dots, y_{ref}(i+N_p|k)]^\top \in \mathbb{R}^{N_p}. \quad (15)$$

By replacing ΔG_k for $\Delta \tilde{G}_k$ and substituting (10) in (13), the cost function J becomes a quadratic and convex function of ΔU_k . Hence, by setting the derivative of J with respect to ΔU_k to zero and solving for ΔU_k , the optimal input sequence that leads to the global minimum of the cost function is found to be

$$\Delta U_k^* = -W^{-1} F (S_x \bar{x}(i|k) + S_g \Delta \tilde{G}_k - Y_{k,ref}), \quad (16)$$

where

$$W = 2(\Psi + S_u^\top \Omega S_u), \quad (17)$$

$$F = 2S_u^\top \Omega. \quad (18)$$

Finally, the control input that is applied to the plant at time $t(i|k)$ is defined as

$$u(i|k) = u(i-1|k) + [1 \quad \mathbf{0}_{1 \times N_p-1}] \Delta U_k^*. \quad (19)$$

Note that all auxiliary matrices that describe the evolution of the states are calculated only once, offline, for $N_p = N_{p,max}$. Subsequently, online, the correctly sized matrices corresponding to the current value of N_p are extracted from the $N_p = N_{p,max}$ matrices. By doing so, the seemingly complicated nonlinear MPC controller simply boils down to plugging information about the states and output reference into a pre-calculated control law. In this way, the algorithm is computationally extremely efficient.

In addition to Q and R_Δ , there are two additional tuning parameters: the MPC sample time $t_{s,in}$ and the outer-loop sample time $t_{s,out}$. First, $t_{s,out}$ is considered. In the proposed framework, the outer-loop sample time is technically the sample time of the outer-loop controller. Throughout literature, there is no general consensus on what would be the best sample time of a digital controller. However, it is self-evident that the sample rate must be sufficiently higher than the desired closed-loop bandwidth. A simple guideline is that the sample time should be at least five times faster than the desired closed-loop bandwidth. Typically, higher sample rates lead to better performance and are therefore preferred. However, in the proposed framework, one must keep in mind that the inner-loop MPC runs at a sample rate which is an integer multiple greater than the outer-loop sample rate, implying that high outer-loop sample rates quickly lead to excessive computational expenses. Therefore, $t_{s,out}$ must be chosen such that it is at least five times

faster than the desired closed-loop bandwidth, preferably more, but at the same time respecting the inner-loop computational burden. Next, $t_{s,in}$ can be selected, considering the relation $N_{p,max} = t_{s,out}/t_{s,in} \in \mathbb{N}$. Again, there is no general consensus on what the best choice is. Typically, when $t_{s,in}$ decreases, reference tracking and disturbance rejection improve up until a certain height where they plateau. This plateauing point is usually adopted for $t_{s,in}$, assuming that the computational effort is reasonable.

From (16) and the schematic overview of the entire framework in Fig. 4, it can be seen that the proposed MPC solution needs the current (and previous) state information in order to calculate the input signal. Whereas only the output is measured, a nonlinear observer is needed to estimate the states of the data-driven model. In this work, state estimation is performed by means of the unscented Kalman filter (UKF), about which the reader is referred to [21–24] for more information.

2.2. Performance quantification and system identification

A nonparametric nonlinearity analysis is performed in order to validate the effectiveness of the proposed framework over the entire specified frequency range of operation, effectively quantifying the performance of the linearisation. The analysis is entirely carried out in the frequency domain, based on the measurement of frequency response functions (FRFs). In this work, we consider excitation signals in the form of random-phase multisines [25]. They are defined as

$$u(t) = \frac{1}{\sqrt{N}} \sum_{q=-N/2+1}^{N/2-1} U_q e^{j(2\pi q f_0 t + \varphi_q)}, \quad (20)$$

with $\varphi_{-q} = -\varphi_q$, $U_{-q} = U_q$, $U_0 = 0$ and with a frequency resolution $f_{res} = f_s/N = 1/T$, where f_s is the sampling frequency and T the period of the multisine. The phases φ_q are independent and uniformly distributed on the interval $[0, 2\pi)$, such that $E\{\varphi_q\} = 0$. Moreover, U_q is the excitation amplitude, j is the imaginary unit and N is the number of time samples, while the division by \sqrt{N} normalises the root-mean-square (RMS) value of the excitation signal. Random-phase multisines are partly deterministic in the frequency domain where their amplitude spectrum can be freely adjusted, but appear like random signals in the time domain.

When it comes to assessing the linearisation performance, multisines are modified such that only odd frequency lines, corresponding to odd values of q , are excited. Moreover, for every group of n_f frequency lines, one line is randomly excluded. This rejected line will serve as an odd detection line measuring odd nonlinear distortions. All the even frequency lines serve as even detection lines, measuring even nonlinear distortions. An illustration of the nonlinear distortion analysis is presented in Fig. 5. In order to reduce the standard deviation of the FRF, the

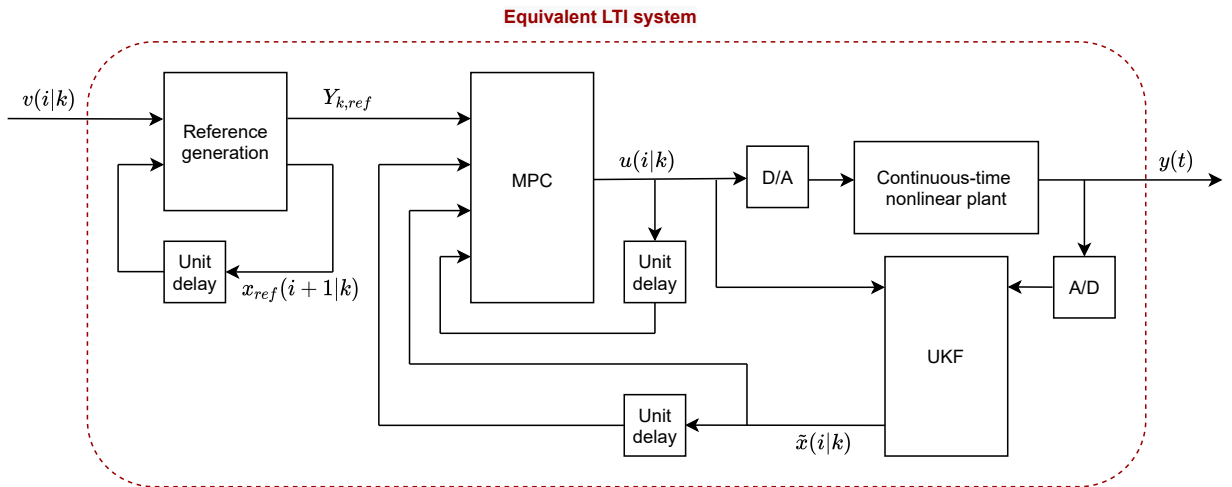


Figure 4: Schematic overview of internal reference tracking framework.

measurements are averaged over R different realisations of P steady-state measurements of the multisine. For more details on the nonlinearity analysis, the reader is referred to [26].

When it comes to nonlinear data-driven modelling, state-space models are obtained through a state-of-the-art identification procedure consisting in 4 steps:

1. *Data collection*: a full multisine, *i.e.*, with no detection line, is applied to the system to be linearised over multiple periods and realisations. Output data are collected and the first few periods of measurement are rejected to suppress transients.
2. *Nonparametric best linear approximation (BLA)*: a nonparametric best linear approximation (BLA) is estimated from the FRF measurements. The nonparametric BLA is found by dividing the averaged discrete Fourier transform (DFT) of the response (output spectrum) by the averaged DFT of the excitation signal (input spectrum). In order to obtain a smooth estimate, a sufficiently high number of realisations and steady-state periods must be processed.
3. *Parametric BLA*: the BLA is parameterised by means of a frequency-domain subspace method [27], weighted by the sample noise covariance matrix of the nonparametric BLA, as in [28]. In this procedure, the model order is a user choice.
4. *Full nonlinear model*: the parametric BLA is used to initialise a least-squares cost function to obtain the full nonlinear model. Here, the E matrix is initially set to zero and the vector of nonlinear output monomials $\zeta(y(k))$ is constructed based on the insight obtained from the nonlinear distortion analysis and engineering judgement.

As for step 3 and 4, results are heavily dependent on the parameters that can be freely chosen. Therefore, in practice, different model orders and basis functions are tested during the identification procedure, after which the combination that provides the best trade-off between model parsimony and flexibility is adopted.

3. Numerical demonstration using a Duffing oscillator

In this section, simulations are performed on a Duffing oscillator with a quadratic and cubic spring nonlinearity. The plant dynamics are governed by

$$m\ddot{y}(t) + c_l\dot{y}(t) + k_ly(t) + k_qy^2(t) + k_cy^3(t) = u(t), \quad (21)$$

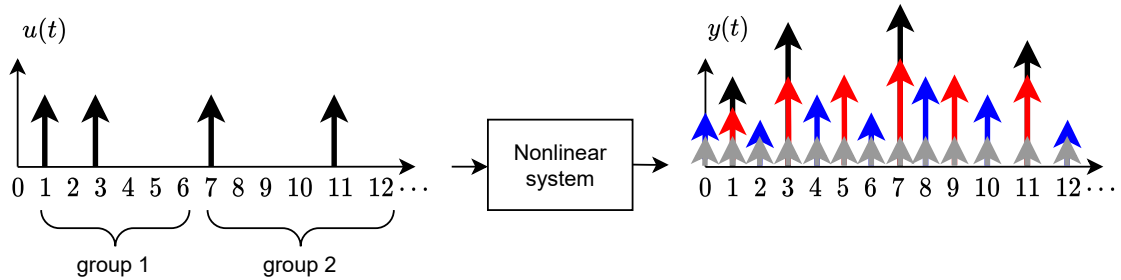


Figure 5: Illustration of the nonlinear distortion analysis. Left: input spectrum of the multisine. Right: the output spectrum with the quantification of the odd (in red) and even (in blue) nonlinear distortions. The grey lines represent the contributions of the disturbing noise and black lines are the linear system response.

	m	c_l	k_l	k_q	k_c
value	1	1	$5 \cdot 10^2$	$5 \cdot 10^4$	$1 \cdot 10^8$
unit	kg	Ns/m	N/m	N/m ²	N/m ³

Table 1: Physical parameters of the nonlinear plant. With these values, the natural frequency and the damping ratio of the underlying linear system are 3.56 Hz and 2.24%, respectively.

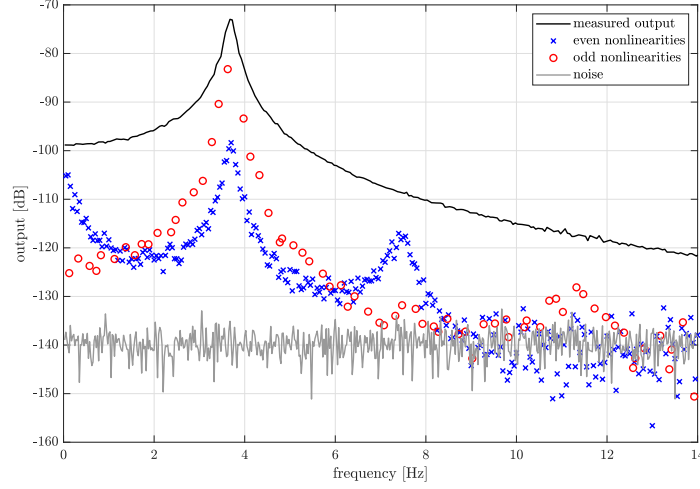


Figure 6: Nonlinear distortion analysis before linearisation.

where m is the mass, c_l is the linear damping coefficient and k_l , k_q and k_c the linear, quadratic and cubic stiffness coefficients, respectively. The output $y(t)$ is the displacement of the mass, and the input $u(t)$ is a force exciting the mass. The system parameters are listed in Table 1.

All simulations are conducted in MATLAB/Simulink. White Gaussian noise is added to the output to simulate sensor inaccuracy with a signal-to-noise ratio (SNR) of 40 dB. From Table 1, it is derived that the linear natural frequency of the system is equal to 3.56 Hz. Based on this, the desired closed-loop bandwidth for an outer-loop controller is chosen equal to 14 Hz, that is well beyond the linear resonance. In other words, the frequency band of interest for the linearising MPC ranges between 0 and 14 Hz. Fig. 6 shows the nonlinear distortion analysis of system (21) before linearisation. It is excited with 10 realisations of 5 periods of an odd random-phase multisine with a RMS amplitude of 0.12 N. For every group of 4 odd frequency lines, 1 line is randomly rejected to serve as an odd detection line. Moreover, 4000 points per period are considered, providing a frequency resolution of 0.025 Hz. The level of odd distortions in this figure (in red) is only 10 dB below the response level around the resonance, translating the strong activation of the nonlinear spring. Even distortions (in blue) are also seen to be non-negligible around 0 Hz, around the nonlinear resonance frequency at 3.8 Hz, and around its second harmonic at 7.6 Hz, as a result of the quadratic spring characteristic.

3.1. System identification

The identification data is obtained by performing 20 realisations of 5 periods of a full random-phase multisine with an RMS amplitude of 0.12 N. The number of data points per period is 40000 at a sampling frequency of 1000 Hz. To ensure steady-state conditions, the first period of every realisation is rejected. Moreover, 1 realisation is saved for validation.

Fig. 7 displays the fitting errors of the parameterised BLA (in orange) and of the full nonlinear model (in green), calculated on validation data. The left plot presents one time-domain period of the validation data with the corresponding linear and nonlinear modelling errors. The nonlinear error (6.64%) appears to be significantly smaller than the linear error (59.2%). These percentages are obtained by dividing the standard deviation of the errors by the standard deviation of the validation output data. The right plot in Fig. 7 shows the same validation data and error signals in the frequency domain. Here, the nonlinear error is consistently one order of magnitude (20 dB) smaller than the output level. The comparison between the error spectra also reveals that the nonlinear model performs well at the resonance and the third harmonic locations, while it does so less convincingly at DC and at the second harmonic location. This

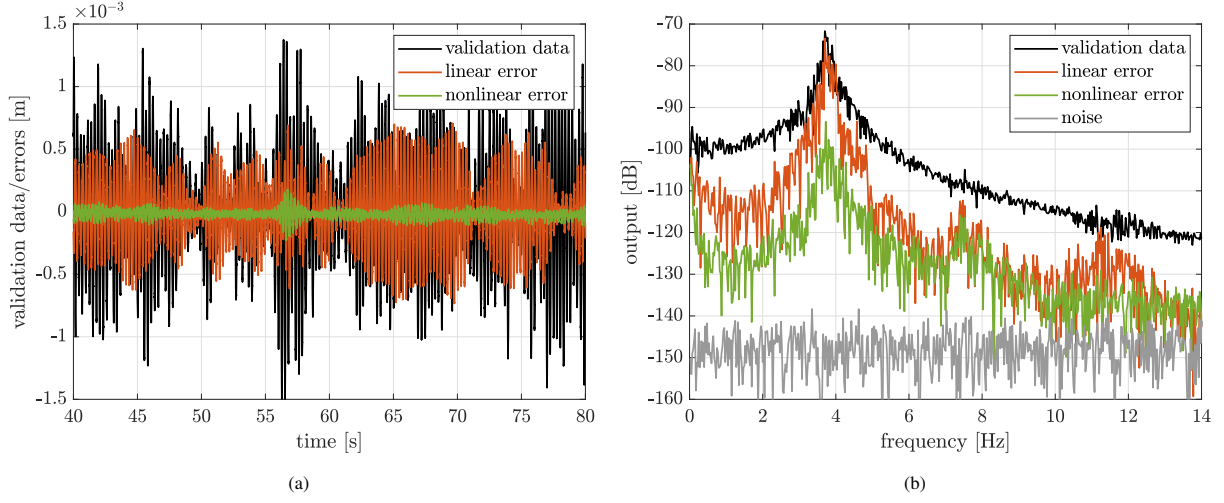


Figure 7: (a) One period of the time-domain validation data and the associated identification errors of the parametric BLA (in orange) and of the nonlinear model (in green). (b) Corresponding frequency-domain validation plot.

is explained by the smaller magnitude of the quadratic nonlinearity in the system compared to the cubic contribution. The parameter values of the obtained second-order state-space model, with $\zeta(y(i|k)) = [y^2(i|k) \ y^3(i|k)]^T$, are provided in Table B.3 of Appendix B.

3.2. Linearisation performance

As stated in Section 2.1, the first important tuning parameter to set is the outer-loop sample time $t_{s,out}$. Since it should be at least 5 times faster than the desired closed-loop bandwidth, it is chosen as $t_{s,out} = 10$ ms. The MPC sample time is set to $t_{s,in} = 1$ ms. The values for Q and R_Δ are chosen as $1 \cdot 10^{12}$ and 1, respectively. As for the UKF, the measurement noise covariance is set to the mean value of the output noise covariance of the nonlinear distortion analysis, *i.e.*, $R_{UKF} = 1.13 \cdot 10^{-14} \text{ m}^2$; the process noise covariance matrix is set to $Q_{UKF} = 0.05 R_{UKF} \mathbf{I}_2$.

Fig. 8 depicts the nonlinear distortion analysis of the linearised plant. The exact same multisine excitation signal as for Fig. 6 is considered. An excellent linearisation is achieved since the odd and even distortions observed Fig. 6 are herein almost coincident with the noise floor. The residual distortions around 3.8 and 7.6 Hz are 50 dB below the validation output. Yet, it must be noted that these residuals can be made arbitrarily close to the noise level by tuning the MPC and UKF parameters more aggressively. However, this would require excessive input energy. For the selected tuning parameters, the outer-loop input $v(i|k)$ and the plant input $u(i|k)$ are shown in Fig. 9 for one period of the multisine. It can be observed from the left subplot that a reasonably large input signal is required to achieve the linearisation. In the right subplot, a zoom-in showing the underlying MPC actions required to achieve linearisation is provided. Seemingly, the most aggressive inputs are calculated at the start of every outer-loop sample period, *i.e.*, when the prediction horizon is at its maximum value, that is $N_{p,max} = t_{s,out}/t_{s,in} = 10$.

3.3. Linearisation robustness

In this section, the robustness of the proposed framework is evaluated first in the case of unmodelled dynamics, and second against extrapolation. In the first test, the quadratic nonlinearity in the system is intentionally not modelled. In the second one, the system is excited at a RMS amplitude that largely exceeds that of the estimation and validation data sets.

3.3.1. Robustness against unmodelled nonlinearities

Fig. 10 displays the nonlinear distortion analysis when only the cubic nonlinearity is considered. This is achieved by setting the first column of the E matrix of the model in Table B.3 to zero. By doing so, the linear part of the model

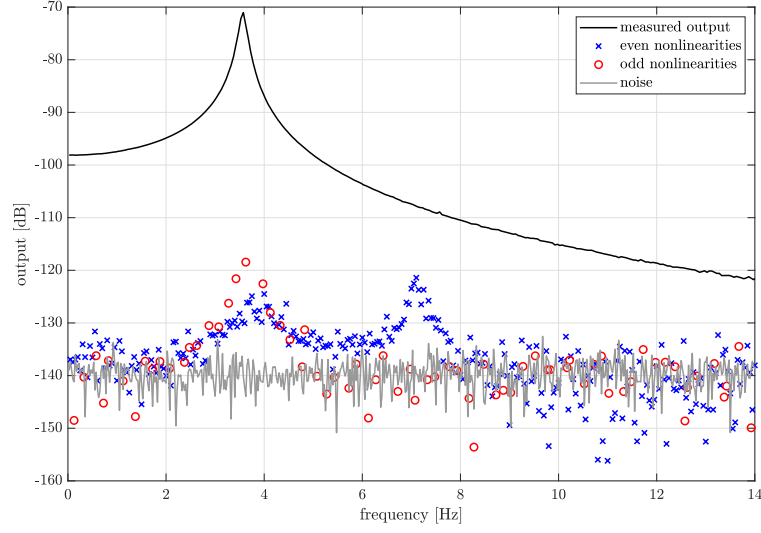


Figure 8: Nonlinear distortion analysis after linearisation. An excellent linearisation is achieved since the odd and even distortions observed Fig. 6 are herein almost coincident with the noise floor.

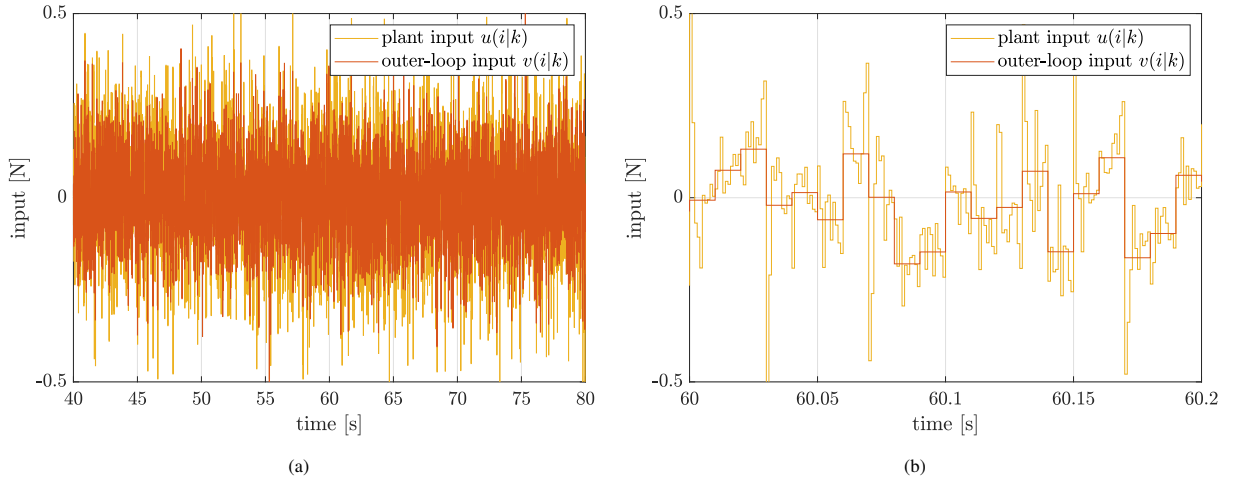


Figure 9: (a) Time-domain inputs during one period of the random-phase multisine and (b) close-up around $t = 60$ s. Both the outer-loop input (in red) and the plant input (in yellow) are shown.

remains exactly the same as in the previous performance test, in this way allowing for a valid comparison between the two. As expected, the even nonlinearities are visibly more present when compared to Fig. 8. In addition, almost no improvement regarding the suppression of the even nonlinearities is noticed when compared to the original system before linearisation in Fig. 6. Only around the resonance frequency, there is a reduction of approximately 15 dB. Nevertheless, the odd nonlinearities are all reduced to a satisfactory level, similarly to Fig. 8. Regarding the even nonlinearities, one could argue that they should in fact be suppressed, even when the quadratic nonlinearity is not modelled. After all, the MPC is tracking the exact same linear reference since the linear parts of both models are the same. So, the integral action property of the MPC should be able to handle the existing modelling errors.

Fig. 11 allows for more insight in the observations drawn from the distortion analysis. Here, two different error signals for both the complete and incomplete models are shown; the left figure presents the MPC error, *i.e.*, the filtered

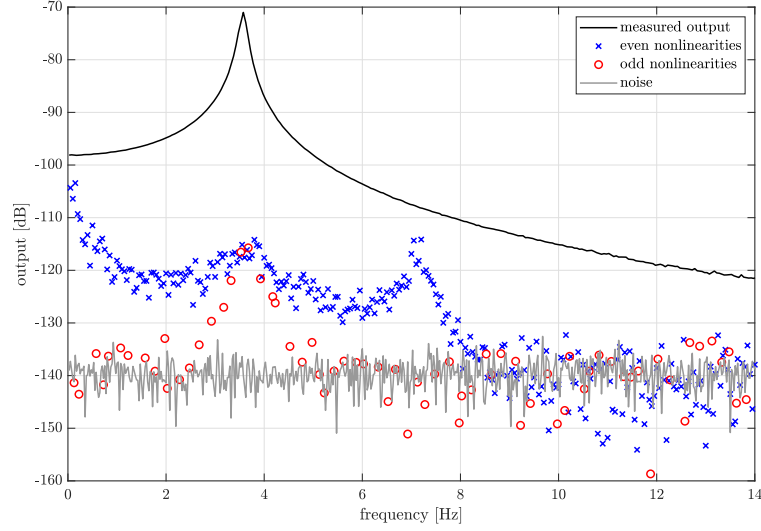


Figure 10: Nonlinear distortion analysis after linearisation in the presence of modelling errors.

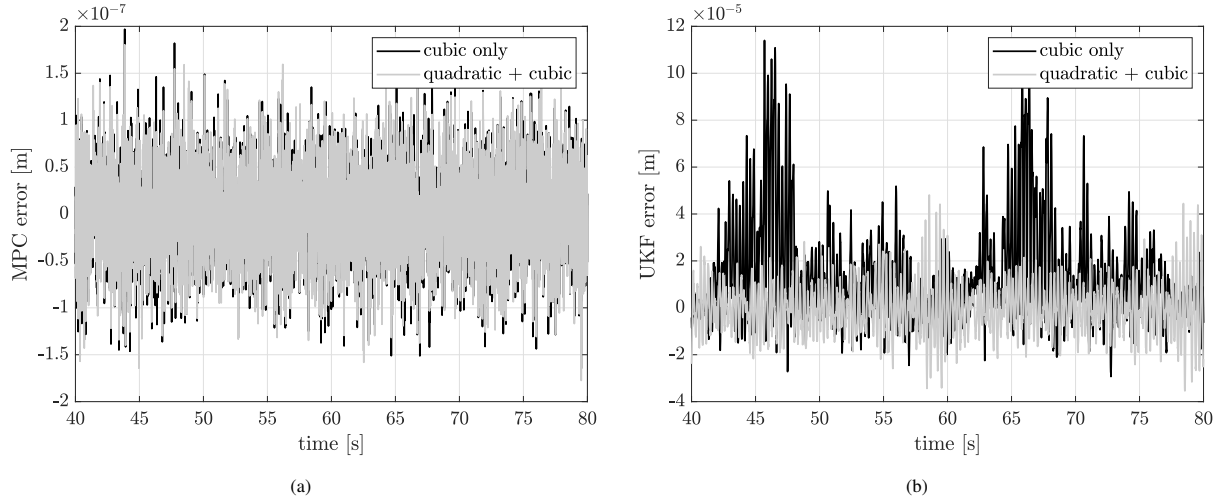


Figure 11: (a) MPC and (b) UKF error plots for one period of the multisine. The errors for the complete (quadratic + cubic, in grey) and incomplete model (cubic only, in black) are shown. The MPC handles modelling errors very well due to its integral action property. On the contrary, the performance of the UKF significantly degrades when the quadratic nonlinearity is not modelled.

output minus the reference output, and the right figure shows the UKF error, *i.e.*, the filtered output minus the true output, the true output being the noise-free output accessible in simulation. It can be seen that there is no noticeable difference between the MPC error signals. Specifically, this means that the MPC is able to match the *filtered* output and the reference output equally well for both the complete and incomplete models. Therefore, it can be concluded that the integral action property of the MPC performs properly. The UKF error plot explains the poor suppression of the even nonlinearities. An increase of the UKF error is noted for the incomplete model. Table 2 gives the RMS values of all the errors and the ratio between these errors and the measured output. Our conclusion from Fig. 11 is confirmed: the MPC is able to track the reference equally well, whereas the UKF error more than doubles. In conclusion, the incomplete model is not able to provide an accurate estimate of the true output, explaining the poor reduction of the even nonlinearities in Fig. 10.

	measured output	MPC error	UKF error
cubic only	$4.14 \cdot 10^{-4}$	$2.27 \cdot 10^{-7}$ (0.0548%)	$2.64 \cdot 10^{-5}$ (6.38%)
quadratic + cubic	$3.82 \cdot 10^{-4}$	$2.22 \cdot 10^{-7}$ (0.0581%)	$1.14 \cdot 10^{-5}$ (2.98%)
extrapolated	$6.51 \cdot 10^{-4}$	$2.36 \cdot 10^{-7}$ (0.0363%)	$2.12 \cdot 10^{-5}$ (3.26%)

Table 2: RMS values (in meter) of the measured output, MPC error and UKF error for the complete and incomplete models (test 1), and the complete model when extrapolated (test 2). The percentages between brackets correspond to the ratios of the errors to the measured output.

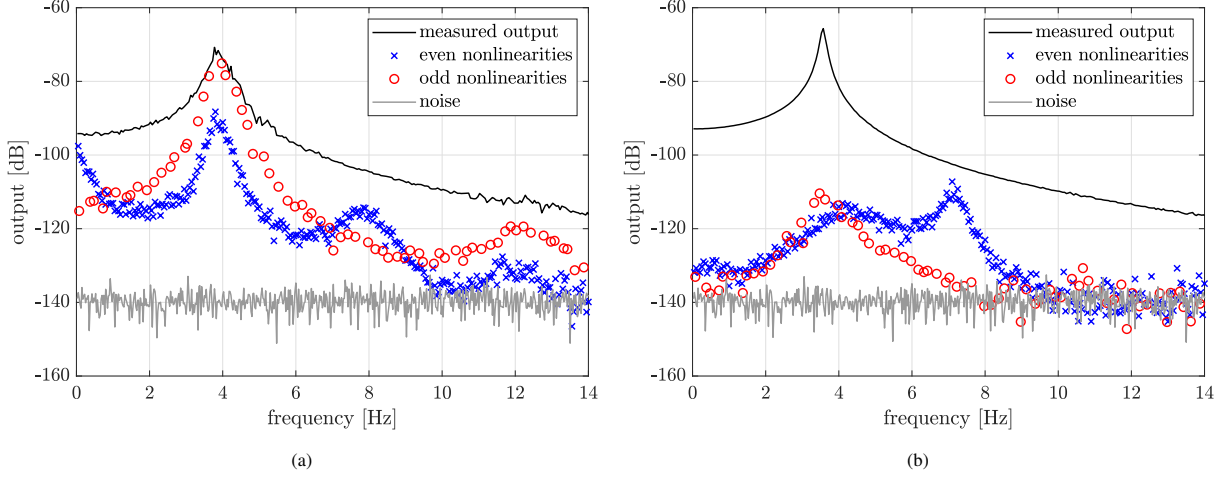


Figure 12: Nonlinear distortion analysis (a) before and (b) after linearisation when excited with a random-phase multisine with a RMS amplitude of 0.22 N.

3.3.2. Robustness against extrapolation

To challenge the extrapolation capability of the control architecture, a random-phase multisine with a RMS amplitude of 0.22 N is used, compared to 0.12 N in the previous sections. Fig. 12 presents the nonlinear distortion analysis (left) before and (right) after linearisation. In the left subfigure, nonlinear distortions are observed to be markedly greater when compared to the analysis in Fig. 6. Nevertheless, a satisfactory linearisation is achieved in the right subplot, the results being similar to Fig. 8, with the peaks around 3.8 and 7.6 Hz slightly amplified.

It is interesting to notice that the low-frequency performance is considerably better than in the case of the model without quadratic nonlinearity in Fig. 10. Again, the MPC and UKF error plots showed in Fig. 13 and tabulated in Table 2 provide more insight. It is seen that the magnitude of the MPC error is similar to the values reported in the previous robustness test, even though the RMS value of the measured output increased by more than 70 percent. This further confirms the excellent working of the integral action property. As expected, the magnitude of the UKF error also increased significantly. Yet, in percent, it compares to the full nonlinear model error. One may then conclude that the poor low-frequency performance in the previous robustness test is due to the nature of the UKF error in Fig. 11. Indeed, there clearly exists an offset in the error signal. From a physical point of view, this offset is explainable since the quadratic nonlinearity is not modelled. In the frequency domain, an offset translates in a non-zero line at 0 Hz. It is therefore coherent that the low-frequency region is mostly affected by the UKF-induced offset.

4. Experimental validation using a prototype of a high-precision motion system

In this section, the proposed control framework is applied to an experimental prototype of a high-precision flexible positioning system, developed for evaluating control strategies. The system, shown in Fig. 14, consists of a lightweight flexible steel beam with dimensions $500 \times 20 \times 2$ mm. The boundary conditions of the beam are realised by means of

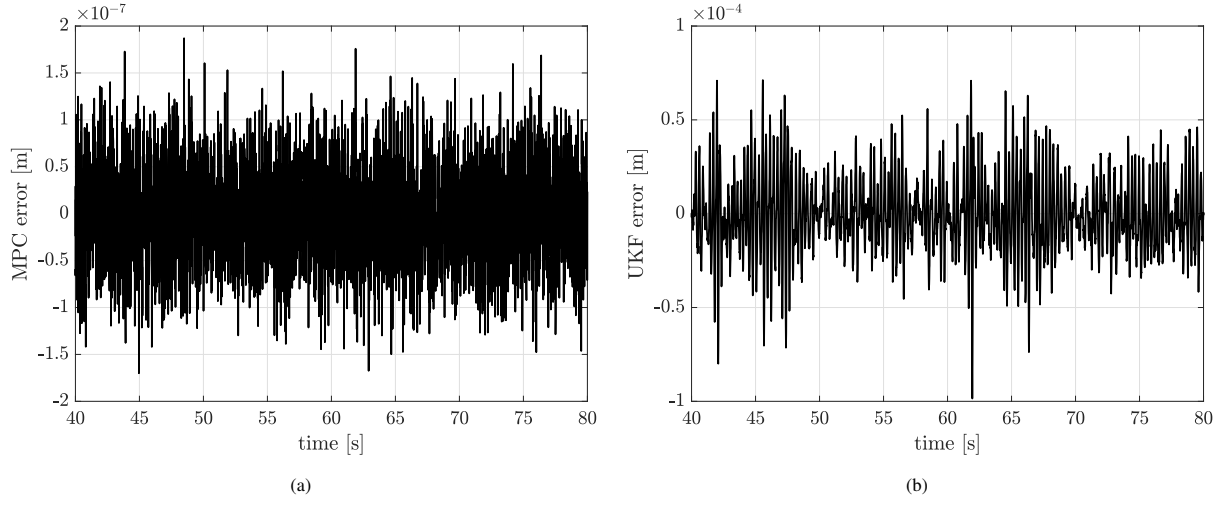


Figure 13: (a) MPC and (b) UKF error plots for one period of a multisine with a RMS amplitude of 0.22 N.

leaf springs, that constrain 4 out of 6 degrees of freedom (DOFs), leaving only one translation and one rotation free. The setup is equipped with 3 collocated sensor-actuator pairs, operating at a sampling frequency of 4096 Hz. The actuators are current-driven voice-coil actuators, whereas the sensors are contactless fiberoptic displacement sensors with an approximate accuracy of $1 \mu\text{m}$. Since the system has more actuators than DOFs, it is said to be over-actuated [29]. However, over-actuation is not considered in this work; in fact, only the middle sensor-actuator pair is exploited. Finally, a positive cubic stiffness, *i.e.*, a hardening spring, is artificially implemented in the setup as is explained in Fig. 15. The value of the spring constant is set to $k_c = 2 \cdot 10^9 \text{ V/m}^3$. By doing so, the obtained dynamics is dominated by the nonlinearity, in the sense that nonlinear distortions under a high-level multisine excitation are less than 10 dB below the linear system dynamics in the first resonance region.

Fig. 16 shows the nonlinear distortion analysis of the system with artificial nonlinearity. It is excited with 5 realisations of 4 periods of an odd random-phase multisine with a RMS amplitude of 0.015 V. For every group of 4 odd frequency lines, 1 line is randomly rejected. Moreover, 3280 points per period are considered at a sampling frequency of 102.4 Hz. In this figure, the resonance around 4 Hz corresponds to a rigid-body mode of the flexible beam, and the resonance around 40 Hz is its first bending mode. Over the entire depicted frequency range, the even

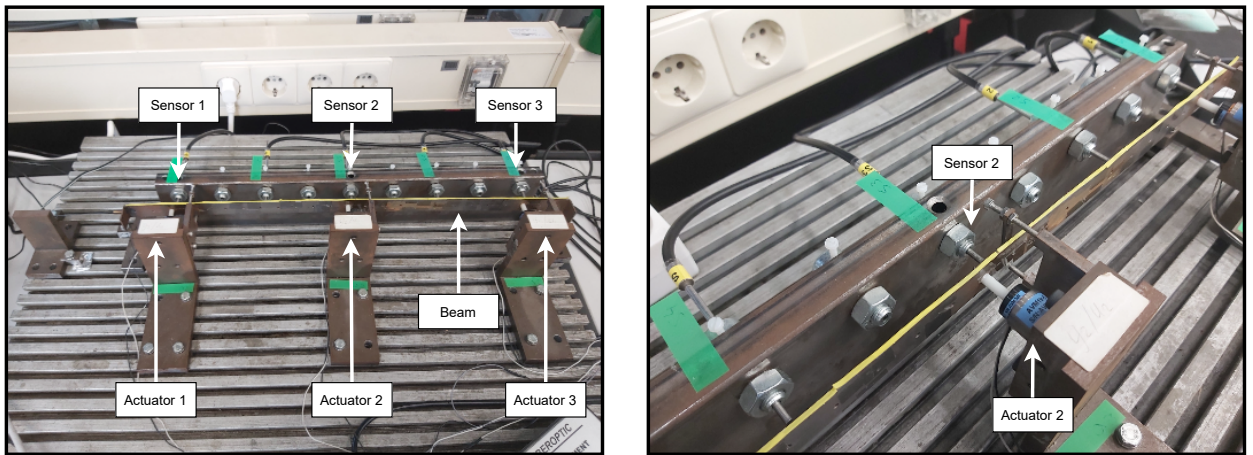


Figure 14: Pictures of the experimental flexible beam setup, equipped with 3 collocated sensor-actuator pairs. In this work, only the middle pair is exploited.

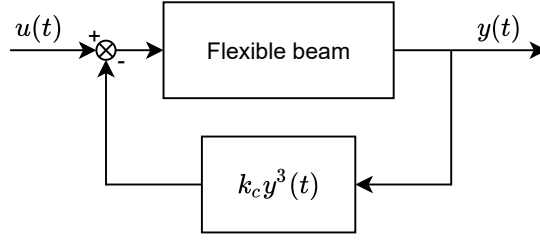


Figure 15: Block diagram of the experimental setup used for validating the proposed framework. A hardening spring is artificially created by feeding back the output sensor measurement, through a cubic function, to the input. The cubic spring constant is set to $k_c = 2 \cdot 10^9 \text{ V/m}^3$.

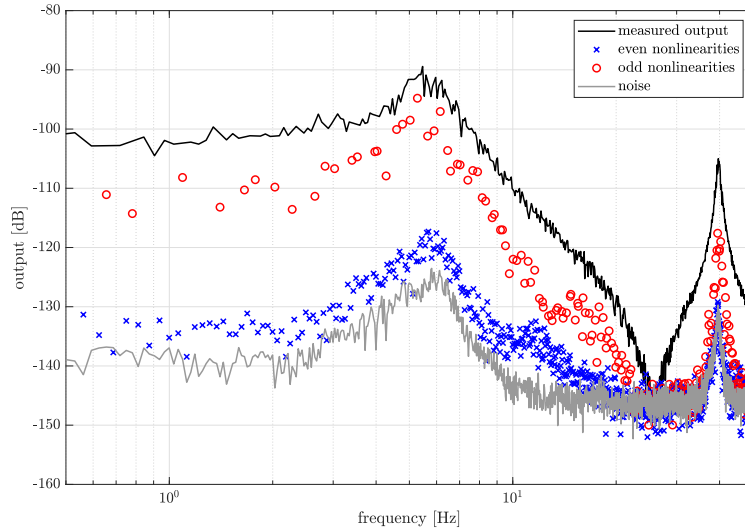


Figure 16: Nonlinear distortion analysis of the system with an artificial nonlinearity created following Fig. 15.

distortions are close to the noise floor, while the odd distortions are never more than one order of magnitude smaller than the measured output.

4.1. System identification

The identification data for the system is obtained by performing 10 realisations of 5 periods of a full random-phase multisine from 0 to 50 Hz and with a RMS amplitude of 0.015 V. The number of data points per period is 16384 at a sampling frequency of 1024 Hz. To ensure steady-state conditions, the first period of every realisation is rejected. One realisation is saved for validation.

Fig. 17 displays the fitting errors of the parameterised BLA (in orange) and of the full nonlinear model (in green), calculated on validation data. The nonlinear model simply embeds a $\zeta(y(t)) = y^3(t)$ monomial; in consequence, the low magnitude even distortions in Fig. 16 are not modelled as they are judged negligible. The left plot of Fig. 17 presents one time-domain period of the validation data with the corresponding linear and nonlinear modelling errors; similar results as in the numerical demonstration in Section 3 are obtained. The nonlinear model reduces the identification error significantly, from 57.4% to 7.34%, when compared to the linear model. In the right subfigure, the validation data is presented in the frequency domain. Up to 15 Hz, the nonlinear error is consistently around 30 dB below the validation output. The parameter values of the obtained nonlinear state-space model are provided in Table B.4 of Appendix B.

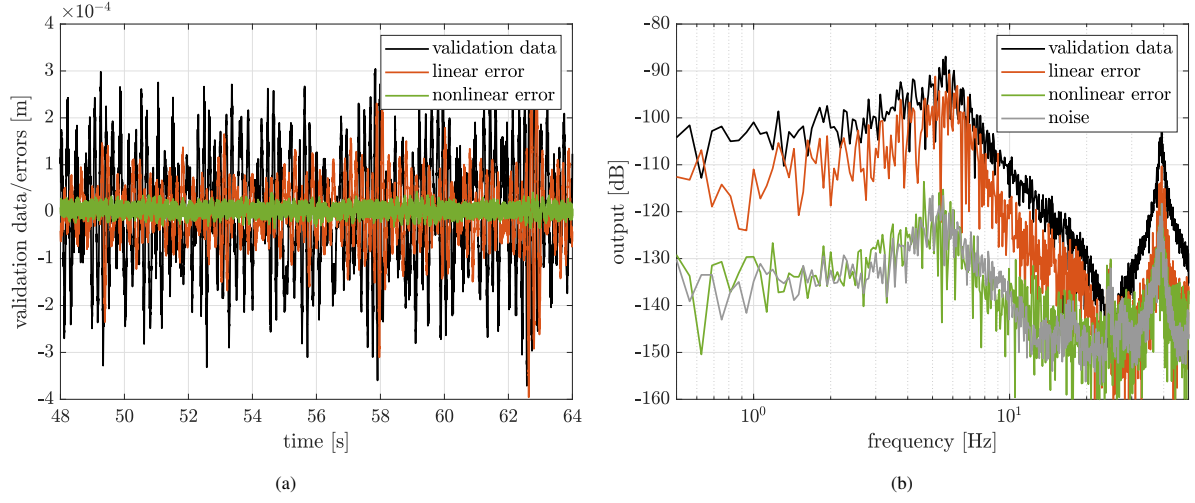


Figure 17: (a) One period of the time-domain validation data and the associated identification errors of the parametric BLA (in orange) and of the nonlinear model (in green). The identification error is reduced from 57.4% to 7.34%. (b) Corresponding frequency-domain validation plot.

4.2. Linearisation performance

In this section, the results of the linearising control framework for both a sine and a random multisine excitation are analysed. The control parameters are chosen following the guidelines discussed in Section 2.1. Here, one must also consider the sampling time of the sensor-actuator pair. Namely, the nonlinear feedback structure of Fig. 15 represents the continuous plant. However, the sensor output is only subtracted from the input at the next time step, considering a sample rate of 4096 Hz. Therefore, the MPC sampling time should be sufficiently higher than $1/4096$ s. While keeping this in mind, the outer-loop sample time is set to $1/102.4$ s. In this way, a desired closed-loop bandwidth of around 20 Hz can be achieved by an outer-loop controller. Next, the sampling time of the MPC is set to $1/512$ s, *i.e.*, 5 times faster than the outer-loop while still sufficiently below $1/4096$ Hz. The values of Q and R_Δ are determined by performing noise-free experiments with the obtained model in simulation; they are set to $3 \cdot 10^8$ and 1, respectively. The values of the covariance matrices of the UKF are tuned on the setup itself. Again, the measurement noise covariance is set to the mean value of the output noise covariance of the nonlinear distortion analysis, *i.e.*, $R_{UKF} = 3.39 \cdot 10^{-15} \text{ m}^2$; the process noise covariance matrix is set to $Q_{UKF} = 10R_{UKF}\mathbf{I}_4$.

Fig. 18 shows the plant input and output when excited by a sine signal. The sine has an amplitude of 0.02 V and a frequency of 2 Hz. The effect of the artificial nonlinear spring is clearly visible in the output plot. The IO behaviour of the linearised plant to the same outer-loop sine excitation is shown in Fig. 19. It can be observed that, in order to track the linear output, the peak amplitudes of the plant input are more than a factor 10 higher than that of the outer-loop sine input. This high amplitude is required to compensate for the severe hardening effect of the spring. The MPC satisfactorily tracks its reference down to an error of 1.05%.

Fig. 20 shows the nonlinear distortion analysis after linearisation. Excellent linearisation is achieved in the first resonance peak range; odd and even distortions are therein located within at most 10 dB of the noise floor. In more details, the odd distortions are eliminated by more than 30 dB, and the even distortions are completely suppressed, even though a cubic nonlinearity only is modelled. As expected, there is no significant performance improvement around the first flexible mode of the beam. As a final performance indicator, Fig. 20 plots the output of the plant before linearisation (in light grey), *i.e.*, the output data in Fig. 16. It is, in this figure, clearly visible that the effect of the hardening spring is eliminated; the resonance peak is shifted back to lower frequencies and the static output value at 0 Hz increases. The colouring of the noise observed in Fig. 16 is also whitened.

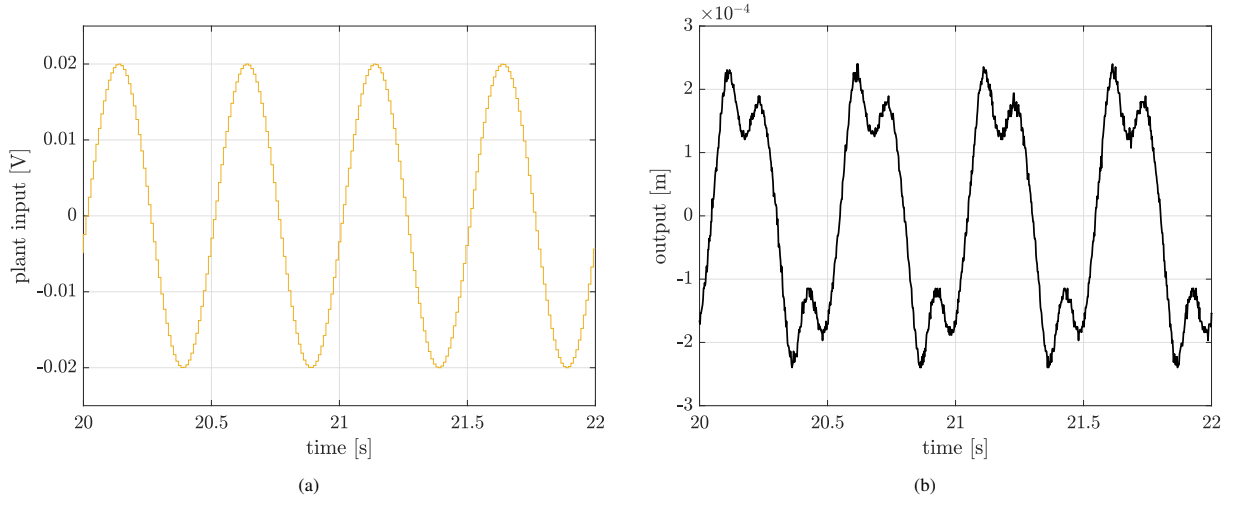


Figure 18: IO data when the original plant is excited by a sine signal with an amplitude of 0.02 V and a frequency of 2 Hz

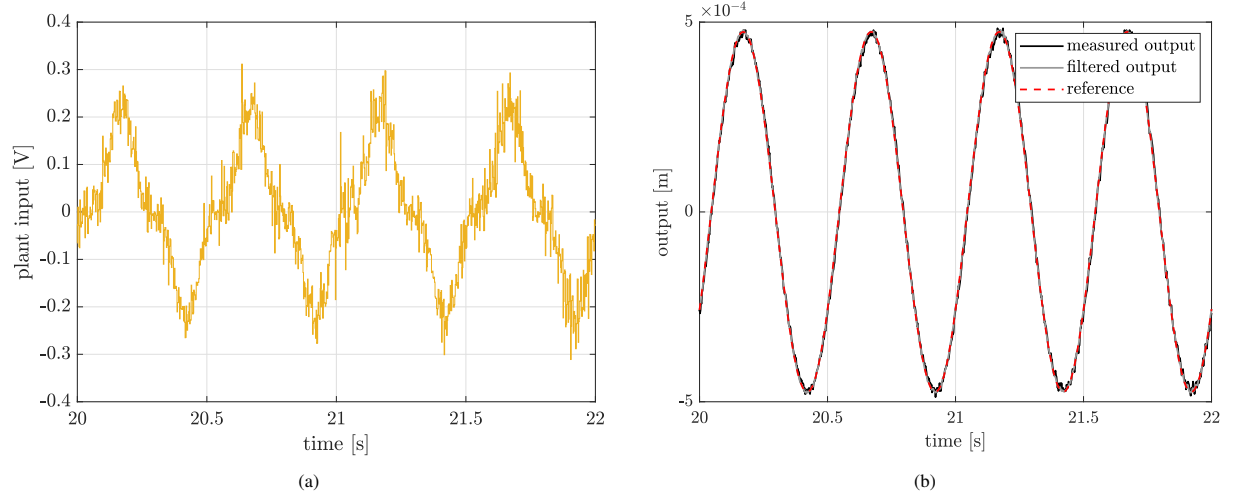


Figure 19: IO data when the controlled plant is excited with the outer-loop sine signal of Fig. 18. Compared to Fig. 18, a significant increase of the plant input amplitude is required to counterbalance the severe hardening effect of the artificial spring.

5. Conclusion

In this paper, a data-driven model predictive control (MPC) approach towards feedback linearisation of nonlinear mechanical systems was presented. The introduced framework is especially designed for nonlinear mechanical systems, but is theoretically applicable to any plant that can be modelled as a linear, time-invariant system with static output nonlinearities in the feedback path. A reference tracking methodology was proposed that eliminates the undesirable nonlinearities, while at the same time preserves the important linear dynamics. Based on a new outer-loop input, an online reference trajectory with time-varying length is generated at every discrete time step. By tracking this reference, the input-output relation between the new outer-loop input and the measured output is governed by the desirable linear part of the nonlinear model.

The dynamic models exploited in this work are identified by exclusively processing experimental data, whereas the tracking problem is solved by means of a model predictive controller, which, due to its integral action property, achieves very low tracking errors. Moreover, by smartly utilising the available reference information, the apparent nonlinear MPC control problem is transformed into a computationally efficient linear optimisation problem with an

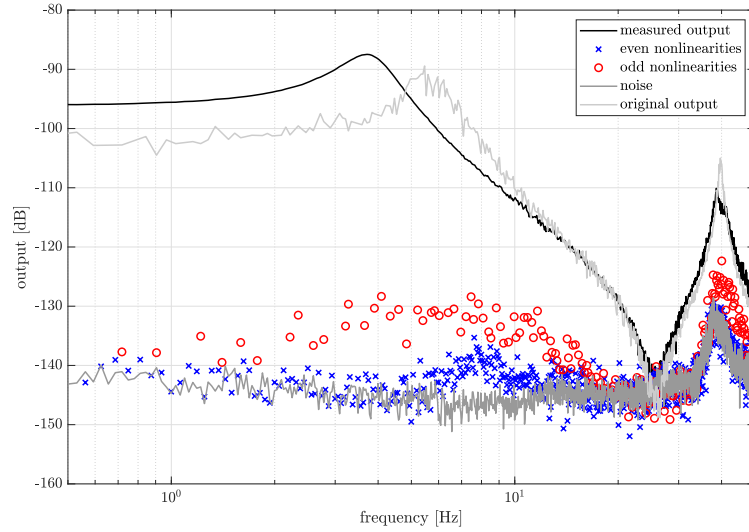


Figure 20: Nonlinear distortion analysis after linearisation, where the odd nonlinearities are significantly suppressed over the primary resonance.

analytical global minimum.

The presented work incorporates all the steps from nonlinear system identification to controller implementation, as well as an intuitive nonparametric nonlinearity analysis. Robustness tests in a realistic simulation environment showed that the MPC controller achieves very low tracking errors when severe modelling errors are present, or when the model is extrapolated outside its fitting region. Here, linearising performance is mainly hampered by the unscented Kalman filter, which relies significantly more on an accurate model. Experimental results on a prototype of a highly nonlinear positioning system confirmed the excellent working of the proposed framework. Suggestions for future research are the extension of the proposed method to the multi-input multi-output case, or to systems that cannot be represented by the model structure in Fig. 2, *e.g.*, systems with input and/or state nonlinearities.

Acknowledgements

This research did not receive any specific grant from funding agencies in the public, commercial, or not-for-profit sectors.

References

- [1] T. Dursun and C. Soutis, "Recent developments in advanced aircraft aluminium alloys," *Materials & Design (1980-2015)*, vol. 56, pp. 862–871, 2014.
- [2] J.-P. Noël and G. Kerschen, "Nonlinear system identification in structural dynamics: 10 more years of progress," *Mechanical Systems and Signal Processing*, vol. 83, pp. 2–35, 2017.
- [3] S. Sastry, *Nonlinear systems: analysis, stability, and control*. Springer Science & Business Media, 2013, vol. 10.
- [4] H. K. Khalil and J. W. Grizzle, *Nonlinear systems*. Prentice hall Upper Saddle River, NJ, 2002, vol. 3.
- [5] D. Wagg and S. Neild, *Nonlinear vibration with control*. Springer, 2016.
- [6] T. Huang, D. Huang, Z. Wang, N. Qin, and A. Shah, "Robust control for a quadrotor uav based on linear quadratic regulator," in *2020 39th Chinese Control Conference (CCC)*. IEEE, 2020, pp. 6893–6898.
- [7] N. Gionfra, H. Siguerdidjane, G. Sandou, D. Faille, and P. Loevenbruck, "Combined feedback linearization and MPC for wind turbine power tracking," in *2016 IEEE Conference on Control Applications (CCA)*. IEEE, 2016, pp. 52–57.
- [8] H. Moradi, A. Alasty, and F. Bakhtiari-Nejad, "Control of a nonlinear boiler-turbine unit using two methods: gain scheduling and feedback linearization," in *ASME International Mechanical Engineering Congress and Exposition*, vol. 43033, 2007, pp. 491–499.
- [9] J.-P. Noël and J. Schoukens, "Grey-box state-space identification of nonlinear mechanical vibrations," *International Journal of Control*, vol. 91, no. 5, pp. 1118–1139, 2018.
- [10] J. A. Rossiter, *Model-based predictive control: a practical approach*. CRC press, 2003.
- [11] E. F. Camacho and C. B. Alba, *Model predictive control*. Springer science & business media, 2013.

- [12] C. E. Garcia, D. M. Prett, and M. Morari, “Model predictive control: theory and practice — a survey,” *Automatica*, vol. 25, no. 3, pp. 335–348, 1989.
- [13] F. Allgöwer and A. Zheng, *Nonlinear model predictive control*. Birkhäuser, 2012, vol. 26.
- [14] G. Papafotiou, J. Kley, K. G. Papadopoulos, P. Bohren, and M. Morari, “Model predictive direct torque control—part ii: implementation and experimental evaluation,” *IEEE Transactions on Industrial Electronics*, vol. 56, no. 6, pp. 1906–1915, 2009.
- [15] J. Rodríguez, R. M. Kennel, J. R. Espinoza, M. Trincado, C. A. Silva, and C. A. Rojas, “High-performance control strategies for electrical drives: an experimental assessment,” *IEEE Transactions on Industrial Electronics*, vol. 59, no. 2, pp. 812–820, 2011.
- [16] P. Cortes, G. Ortiz, J. I. Yuz, J. Rodríguez, S. Vazquez, and L. G. Franquelo, “Model predictive control of an inverter with output LC filter for UPS applications,” *IEEE Transactions on Industrial Electronics*, vol. 56, no. 6, pp. 1875–1883, 2009.
- [17] H. Miranda, P. Cortés, J. I. Yuz, and J. Rodríguez, “Predictive torque control of induction machines based on state-space models,” *IEEE Transactions on Industrial Electronics*, vol. 56, no. 6, pp. 1916–1924, 2009.
- [18] A. H. González, E. J. Adam, and J. L. Marchetti, “Conditions for offset elimination in state space receding horizon controllers: A tutorial analysis,” *Chemical Engineering and Processing: Process Intensification*, vol. 47, no. 12, pp. 2184–2194, 2008.
- [19] L. Wang, “A tutorial on model predictive control: Using a linear velocity-form model,” *Developments in Chemical Engineering and Mineral Processing*, vol. 12, no. 5-6, pp. 573–614, 2004.
- [20] G. Betti, M. Farina, and R. Scattolini, “A robust MPC algorithm for offset-free tracking of constant reference signals,” *IEEE Transactions on Automatic Control*, vol. 58, no. 9, pp. 2394–2400, 2013.
- [21] S. J. Julier, J. K. Uhlmann, and H. F. Durrant-Whyte, “A new approach for filtering nonlinear systems,” in *Proceedings of 1995 American Control Conference-ACC’95*, vol. 3. IEEE, 1995, pp. 1628–1632.
- [22] S. J. Julier and J. K. Uhlmann, “New extension of the Kalman filter to nonlinear systems,” in *Signal processing, sensor fusion, and target recognition VI*, vol. 3068. International Society for Optics and Photonics, 1997, pp. 182–193.
- [23] E. A. Wan and R. Van Der Merwe, “The unscented Kalman filter for nonlinear estimation,” in *Proceedings of the IEEE 2000 Adaptive Systems for Signal Processing, Communications, and Control Symposium (Cat. No. 00EX373)*. Ieee, 2000, pp. 153–158.
- [24] J. J. LaViola, “A comparison of unscented and extended Kalman filtering for estimating quaternion motion,” in *Proceedings of the 2003 American Control Conference, 2003.*, vol. 3. IEEE, 2003, pp. 2435–2440.
- [25] J. Schoukens and L. Ljung, “Nonlinear system identification: A user-oriented road map,” *IEEE Control Systems Magazine*, vol. 39, no. 6, pp. 28–99, 2019.
- [26] J. Schoukens, M. Vaes, and R. Pintelon, “Linear system identification in a nonlinear setting: nonparametric analysis of the nonlinear distortions and their impact on the best linear approximation,” *IEEE Control Systems Magazine*, vol. 36, no. 3, pp. 38–69, 2016.
- [27] T. McKelvey, H. Akçay, and L. Ljung, “Subspace-based multivariable system identification from frequency response data,” *IEEE Transactions on Automatic Control*, vol. 41, no. 7, pp. 960–979, 1996.
- [28] R. Pintelon, “Frequency-domain subspace system identification using non-parametric noise models,” *Automatica*, vol. 38, no. 8, pp. 1295–1311, 2002.
- [29] K. Classens, W. Heemels, and T. Oomen, “A closed-loop perspective on fault detection for precision motion control: With application to an overactuated system,” in *2021 IEEE International Conference on Mechatronics (ICM)*. IEEE, 2021, pp. 1–6.

Appendix A. Derivation of the MPC prediction matrices

This appendix concerns the derivation of the MPC prediction matrices, which are used to describe the evolution of the states and output over the prediction horizon. Remember the relations $t(0|k) = t(k) \in \mathbb{R}_{\geq 0}$, $\bar{x}(0|k) = \bar{x}(k) \in \mathbb{R}^n$, $\Delta u(0|k) = \Delta u(k) \in \mathbb{R}$ and $\Delta \zeta(y(0|k)) = \Delta \zeta(y(k)) \in \mathbb{R}^s$. Based on the augmented state-space (8), the N_p future predictions of the output at time $t(k)$, *i.e.*,

$$Y_k = \left[y(i+1|k), \dots, y(i+N_p|k) \right]^\top, \quad (\text{A.1})$$

are given by the following relations

$$\begin{cases}
\bar{x}(1|k) &= \bar{A}\bar{x}(k) + \bar{B}\Delta u(k) + \bar{E}\Delta\zeta(y(k)) \\
y(1|k) &= \bar{C}\bar{x}(1|k) \\
&= \bar{C}\bar{A}\bar{x}(k) + \bar{C}\bar{B}\Delta u(k) + \bar{C}\bar{E}\Delta\zeta(y(k)), \\
\bar{x}(2|k) &= \bar{A}\bar{x}(1|k) + \bar{B}\Delta u(1|k) + \bar{E}\Delta\zeta(y(1|k)) \\
&= \bar{A}^2\bar{x}(k) + \bar{A}\bar{B}\Delta u(k) + \bar{A}\bar{E}\Delta\zeta(y(k)) + \bar{B}\Delta u(1|k) + \bar{E}\Delta\zeta(y(1|k)) \\
y(2|k) &= \bar{C}\bar{x}(2|k) \\
&= \bar{C}\bar{A}^2\bar{x}(k) + \bar{C}\bar{A}\bar{B}\Delta u(k) + \bar{C}\bar{A}\bar{E}\Delta\zeta(y(k)) + \bar{C}\bar{B}\Delta u(1|k) \\
&\quad + \bar{C}\bar{E}\Delta\zeta(y(1|k)), \\
&\vdots \\
\bar{x}(N_p|k) &= \bar{A}\bar{x}(N_p - 1|k) + \bar{B}\Delta u(N_p - 1|k) + \bar{E}\Delta\zeta(y(N_p - 1|k)) \\
&= \bar{A}^{N_p}\bar{x}(k) + \bar{A}^{N_p-1}\bar{B}\Delta u(k) + \bar{A}^{N_p-1}\bar{E}\Delta\zeta(y(k)) \\
&\quad + \dots + \bar{A}\bar{B}\Delta u(N_p - 2|k) + \bar{A}\bar{E}\Delta\zeta(y(N_p - 2|k)) + \bar{B}\Delta u(N_p - 1|k) \\
&\quad + \bar{E}\Delta\zeta(y(N_p - 1|k)) \\
y(N_p|k) &= \bar{C}\bar{x}(N_p|k) \\
&= \bar{C}\bar{A}^{N_p}\bar{x}(k) + \bar{C}\bar{A}^{N_p-1}\bar{B}\Delta u(k) + \bar{C}\bar{A}^{N_p-1}\bar{E}\Delta\zeta(y(k)) \\
&\quad + \dots + \bar{C}\bar{A}\bar{B}\Delta u(N_p - 2|k) + \bar{C}\bar{A}\bar{E}\Delta\zeta(y(N_p - 2|k)) \\
&\quad + \bar{C}\bar{B}\Delta u(N_p - 1|k) + \bar{C}\bar{E}\Delta\zeta(y(N_p - 1|k)),
\end{cases} \tag{A.2}$$

which can be cast into a more compact form as follows

$$Y_k = S_x \bar{x}(k) + S_u \Delta U_k + S_g \Delta G_k. \tag{A.3}$$

where

$$S_x = \begin{bmatrix} \bar{C}\bar{A} \\ \bar{C}\bar{A}^2 \\ \vdots \\ \bar{C}\bar{A}^{N_p} \end{bmatrix}; \quad S_u = \begin{bmatrix} \bar{C}\bar{B} & 0 & \dots & 0 \\ \bar{C}\bar{A}\bar{B} & \bar{C}\bar{B} & \dots & 0 \\ \vdots & \vdots & \ddots & \vdots \\ \bar{C}\bar{A}^{N_p-1}\bar{B} & \bar{C}\bar{A}^{N_p-2}\bar{B} & \dots & \bar{C}\bar{B} \end{bmatrix}; \quad S_g = \begin{bmatrix} \bar{C}\bar{E} & \mathbf{0}_{1 \times s} & \dots & \mathbf{0}_{1 \times s} \\ \bar{C}\bar{A}\bar{E} & \bar{C}\bar{E} & \dots & \mathbf{0}_{1 \times s} \\ \vdots & \vdots & \ddots & \vdots \\ \bar{C}\bar{A}^{N_p-1}\bar{E} & \bar{C}\bar{A}^{N_p-2}\bar{E} & \dots & \bar{C}\bar{E} \end{bmatrix}, \tag{A.4}$$

and

$$\Delta U_k = \begin{bmatrix} \Delta u(k) \\ \Delta u(1|k) \\ \vdots \\ \Delta u(N_p - 1|k) \end{bmatrix}; \quad \Delta G_k = \begin{bmatrix} \Delta\zeta(y(k)) \\ \Delta\zeta(y(1|k)) \\ \vdots \\ \Delta\zeta(y(N_p - 1|k)) \end{bmatrix}. \tag{A.5}$$

Ultimately, ΔU_k is the vector to be optimised while $\bar{x}(k)$ is constructed from output measurements and ΔG_k is known (or estimated, technically) in advance. The obtained relations can be generalised to any time $t(i|k)$ and for any length of the prediction horizon N_p .

Appendix B. Nonlinear state-space parameter values

This appendix provides the parameter values of the two nonlinear state-space models derived in the paper. Table B.3 corresponds to the simulation experiments in Section 3, and Table B.4 details the model of the experimental setup in Section 4.

Parameter	Value	Parameter	Value	Parameter	Value
$A(1, 1)$	$9.992 \cdot 10^{-1}$	$B(1, 1)$	$-2.468 \cdot 10^{-3}$	$E(1, 1)$	$1.326 \cdot 10^2$
$A(2, 1)$	$-2.070 \cdot 10^{-2}$	$B(2, 1)$	$2.916 \cdot 10^{-4}$	$E(2, 1)$	7.221
$A(1, 2)$	$2.428 \cdot 10^{-2}$	$C(1, 1)$	$2.467 \cdot 10^{-3}$	$E(1, 2)$	$2.598 \cdot 10^5$
$A(2, 2)$	$9.994 \cdot 10^{-1}$	$C(1, 2)$	$1.854 \cdot 10^{-2}$	$E(2, 2)$	$-4.306 \cdot 10^4$

Table B.3: Second-order discrete-time state-space parameters of the full simulation model ($t_s = 1/1000$ s).

Parameter	Value	Parameter	Value	Parameter	Value
$A(1, 1)$	$9.739 \cdot 10^{-1}$	$A(3, 3)$	1.001	$C(1, 1)$	$-1.297 \cdot 10^{-2}$
$A(2, 1)$	$-2.270 \cdot 10^{-1}$	$A(4, 3)$	$1.393 \cdot 10^{-2}$	$C(1, 2)$	$1.534 \cdot 10^{-3}$
$A(3, 1)$	$-4.9715 \cdot 10^{-4}$	$A(1, 4)$	$9.026 \cdot 10^{-4}$	$C(1, 3)$	$-5.293 \cdot 10^{-2}$
$A(4, 1)$	$-7.984 \cdot 10^{-4}$	$A(2, 4)$	$-2.339 \cdot 10^{-2}$	$C(1, 4)$	$9.680 \cdot 10^{-3}$
$A(1, 2)$	$2.421 \cdot 10^{-1}$	$A(3, 4)$	$-3.508 \cdot 10^{-2}$	$E(1, 1)$	$2.245 \cdot 10^6$
$A(2, 2)$	$9.631 \cdot 10^{-1}$	$A(4, 4)$	$9.913 \cdot 10^{-1}$	$E(2, 1)$	$7.039 \cdot 10^6$
$A(3, 2)$	$5.329 \cdot 10^{-3}$	$B(1, 1)$	$1.287 \cdot 10^{-3}$	$E(3, 1)$	$-2.326 \cdot 10^6$
$A(4, 2)$	$-4.458 \cdot 10^{-3}$	$B(2, 1)$	$-3.121 \cdot 10^{-3}$	$E(4, 1)$	$-1.112 \cdot 10^7$
$A(1, 3)$	$-7.025 \cdot 10^{-3}$	$B(3, 1)$	$1.750 \cdot 10^{-3}$		
$A(2, 3)$	$-8.304 \cdot 10^{-3}$	$B(4, 1)$	$5.684 \cdot 10^{-3}$		

Table B.4: Fourth-order discrete-time state-space parameters of the experimental setup ($t_s = 1/1024$ s).